EUROPEAN ORGANIZATION FOR NUCLEAR RESEARCH

L3 Note 2576
July 7, 2000

Search for Production of Neutral Higgs Scalars in e^+e^- Annihilations at LEP

L3 Collaboration

Abstract

Using data collected at centre-of-mass energies between 189 and 202 GeV corresponding to an integrated luminosity of 410 pb^{-1}, the production of Higgs like scalars, either in association with a Z or in pairs, is searched for. No signal is found. Limits on the couplings are set depending on the mass of the scalars.

Submitted to the *XXXth International Conference on High Energy Physics*
July 27 - August 2, 2000, Osaka, Japan

Introduction

In the Standard Model (SM) [1] particles acquire mass due to spontaneous symmetry breaking by introducing one scalar doublet field. The so called Higgs mechanism [2] leads to one remnant scalar particle, the Higgs boson. The mass of the Higgs boson is not predicted, and so far, no evidence for this particle is seen. More general models [3], e.g. supersymmetric ones, need at least two scalar doublets for the generation of particle masses. After symmetry breaking five scalar bosons appear, two CP even scalars h and H, one CP odd scalar A and two charged scalars $H^{\pm}$. In this paper a search for the production of h in the process $e^+e^- \to hZ$ and of hA in the process $e^+e^- \to hA$ in several final states is performed and scalar couplings to the Z boson are probed.

Parametrisation of the production cross sections

The dominant production mechanisms are shown in the following graphs:

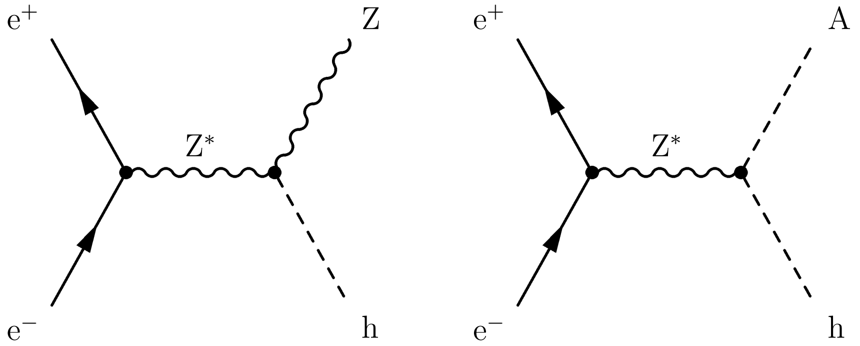

The cross sections for the production of the hZ and hA final states, respectively, can be written [3]:

$$\sigma_{\mathrm{hZ}} = \rho \cdot \sigma_{\mathrm{hZ}}^{SM} \tag{1}$$

$$\sigma_{\mathrm{hA}} = \eta\lambda \cdot \sigma_{\nu\nu}^{SM} \tag{2}$$

with

$$\rho = \frac{g_{\mathrm{hZZ}}^2}{(g_{\mathrm{hZZ}}^{SM})^2} \tag{3}$$

$$\eta = \frac{g_{\mathrm{hAZ}}^2}{(g_{\mathrm{Z}\nu\nu}^{SM})^2}. \tag{4}$$

The couplings g_{hZZ} and g_{hAZ} are probed, g_{hZZ}^{SM} and $g_{\mathrm{Z}\nu\nu}^{SM}$ are the hZZ and $\mathrm{Z}\nu\nu$ couplings in the SM, respectivlely, $\sigma_{\mathrm{hZ}}^{SM}$ and $\sigma_{\nu\nu}^{SM}$ the cross sections for $e^+e^- \to hZ$ and $e^+e^- \to \nu\nu$ in the SM, and λ is a phase space factor accounting for the p-wave threshold behaviour. In the Two Higgs Doublet Model ρ and η are related to $\tan\beta$, the ratio of vacuum expectation values of Higgs superfields, and the Higgs mixing angle α as $\rho = \sin^2(\beta - \alpha)$ and $\eta = \cos^2(\beta - \alpha)$.

Data and Monte Carlo Samples

Data taken by the L3 detector [4] at center-of-mass energies ranging from 189 to 202 GeV are analysed. The luminosities collected at each center-of-mass energy are reported in Table 1.

The cross sections of process $e^+e^- \rightarrow hZ$ in the SM is calculated using the HZHAv3.0 generator [5]. For studies of the efficiencies for $e^+e^- \rightarrow hZ$ and $e^+e^- \rightarrow hA$ Monte Carlo samples are generated using PYTHIA [6] and HZHA. For the background studies, the following Monte Carlo programs are used: PYTHIA ($e^+e^- \rightarrow q\bar{q}(\gamma)$), KORALW [7] ($e^+e^- \rightarrow W^+W^-$), KORALZ [8] ($e^+e^- \rightarrow \tau^+\tau^-$), PYTHIA and PHOJET [9] ($e^+e^- \rightarrow e^+e^-q\bar{q}$), EXCALIBUR [10] ($e^+e^- \rightarrow f\bar{f}'f''\bar{f}'''$) and PYTHIA ($e^+e^- \rightarrow ZZ$ and $e^+e^- \rightarrow Ze^+e^-$).

The L3 detector response is simulated using the GEANT 3.15 program [11], which takes into account the effects of energy loss, multiple scattering and showering in the detector. The GHEISHA program [12] is used to simulate hadronic interactions in the detector.

Analysis of $e^+e^- \rightarrow hZ$

The hZ $\rightarrow b\bar{b}f\bar{f}$ final state

The search is performed in the channels $hZ \rightarrow b\bar{b}q\bar{q}$, $hZ \rightarrow b\bar{b}\nu\nu$, $hZ \rightarrow b\bar{b}\ell^+\ell^-$, where ℓ is an electron, a muon or a tau, and in $hZ \rightarrow \tau^+\tau^-q\bar{q}$. The analysis procedure is the same as described in Ref. [13]. In the mass range investigated, between 60 GeV and 110 GeV, no signal is observed. Assuming that the branching fractions of h are like predicted in the SM, upper limits of the parameter ρ are derived as function of M_h and shown in Figure 1. The exclusion contour crosses the $\rho = 1$ line at $M_h = 106.7$ GeV, reproducing the result of the SM Higgs search.

The hZ $\rightarrow q\bar{q}f\bar{f}$ final states

The process $e^+e^- \rightarrow hZ$ is searched for in the final states $hZ \rightarrow q\bar{q}q\bar{q}$, $hZ \rightarrow q\bar{q}\ell^+\ell^-$, where ℓ is an electron, a muon or a tau, and $hZ \rightarrow q\bar{q}\nu\nu$. The preselection for the different channels is similar to Ref. [13]. Event candidates of the $hZ \rightarrow q\bar{q}q\bar{q}$ final state are characterised by high multiplicity and a four jet topology. The $hZ \rightarrow q\bar{q}\ell^+\ell^-$ final states must have two electrons, muons or taus and two hadronic jets. A kinematic fit imposing energy momentum conservation is applied to the events. Furthermore the invariant mass of the two leptons or of the two jets stemming from the Z decay are constrained to the Z mass. The distributions of the invariant mass of the two jets assumed to originate from the decay of the h are shown for each of the Z decay channels in Figure 2. No signal is observed. The main background contributions are $e^+e^- \rightarrow W^+W^-$ for the $hZ \rightarrow q\bar{q}q\bar{q}$ final state and $e^+e^- \rightarrow ZZ$ for the others. Events of the $hZ \rightarrow q\bar{q}\nu\nu$ final state are characterised by two acoplanar hadronic jets and missing energy. A neural network is used to separate them from SM background, which is dominated by $e^+e^- \rightarrow W^+W^-$ with one W decaying into hadrons and the other into leptons. The dijet mass, calculated with the constraint that the missing mass equals the mass of the Z boson, is shown in Figure 3 for data[1)], the SM background, and the expectation of a signal from h with $m_h = 80$ GeV.

Systematic uncertainties are treated as in Ref. [13]. A limit is derived on the parameter ρ, assuming a branching fraction of h into hadrons as predicted in the SM, as function of M_h.

[1)] in this analysis only data from centre-of-mass energies between 192 and 202 GeV are used

This is shown in Figure 4. Assuming the SM coupling for g_{hZZ} a mass of h below 94.8 GeV is excluded.

Analysis of $\mathrm{e^+e^-} \rightarrow$ hA

The search for $\mathrm{e^+e^-} \rightarrow \mathrm{hA}$ is done with the assumptions that both h and A decay either dominantly into $\mathrm{b\bar{b}}$ or $\mathrm{q\bar{q}}$ or one of them into $\mathrm{b\bar{b}}$ or $\mathrm{q\bar{q}}$ and the other into $\tau^+\tau^-$. The mass ranges $M_\mathrm{h} \geq 50$ GeV and $M_\mathrm{A} \geq 50$ GeV are considered. Systematic uncertainties in the following analyses are taken into account as described in Ref. [14].

The hA $\rightarrow \mathrm{b\bar{b}b\bar{b}}$ final state

High multiplicity events which are energetically balanced are selected. Four jets and no high energetic leptons or photons are required. The event selection follows the procedure described in Ref. [14]. Then a kinematic fit is applied to events imposing the energy and momentum constraints and determinating the invariant masses of the three possible combinations to assign four jets to two parent particles. The obtained dijet masses are compared to the $(M_\mathrm{h}, M_\mathrm{A})$ hypothesis under study and the pairing with the best χ^2 is chosen. The χ^2 probability together with the probability that the events contain jets originating from b quarks are combined to a discriminant. The distribution of this discriminant is shown in Figure 5. The data are in good agreement with the expectation from SM background, which mainly results from $\mathrm{e^+e^-} \rightarrow \mathrm{W^+W^-}$, $\mathrm{e^+e^-} \rightarrow \mathrm{ZZ}$ and $\mathrm{e^+e^-} \rightarrow \mathrm{q\bar{q}}(\gamma)$. Exclusion limits are derived in the $(M_\mathrm{H}, M_\mathrm{A})$ plane for parameter η' defined as a product of cross section scale factor η (see equation 4) and branching fraction $\mathcal{B}(\mathrm{hA} \rightarrow \mathrm{b\bar{b}b\bar{b}})$ $\eta' = \eta \cdot \mathcal{B}(\mathrm{hA} \rightarrow \mathrm{b\bar{b}b\bar{b}})$. The result is shown in Figure 6 for $\eta' = 1$ and $\eta' = 0.5$. The upper limit on η' as function of $(M_\mathrm{H} + M_\mathrm{A})/2$ is shown in Figure 7 for $M_\mathrm{h} = M_\mathrm{A}$. At $\eta' = 1$ a mass lower limit for M_h and M_A of 88 GeV is derived.

The hA $\rightarrow \mathrm{q\bar{q}q\bar{q}}$ final state

The selection of $\mathrm{hA} \rightarrow \mathrm{q\bar{q}q\bar{q}}$ again requires high multiplicity and energetically balanced events. The Durham clustering algorithm is used to force the events into four jets. A neural net is applied to kinematical and topological quantities like y_{34}, the value of the cut parameter when the event changes from three to four jet topology, the event spherocity, the energy of the least energetic jet and the polar angle of the dijet combination assigned to the h. The neural net ouput value discriminates between signal and background from SM processes.

For signal-like events a kinematic fit is performed requiring energy momentum conservation. For all jet pairings an additional constrained is applied by the following requirement on the dijet invariant masses for a given hypothesis of the scalar masses, M_A and M_h: $M_{\mathrm{q\bar{q}}} - M_{\mathrm{q'\bar{q}'}} = M_\mathrm{A} - M_\mathrm{h}$ The final variable is defined as half of the sum of the dijet masses obtained from the fit with the best χ^2, $\frac{1}{2}(M_{\mathrm{q\bar{q}}} + M_{\mathrm{q'\bar{q}'}})$, which is shown in Figure 8 for data and SM backgrounds, which consist mainly of $\mathrm{e^+e^-} \rightarrow \mathrm{W^+W^-}$. The two distributions correspond to $M_\mathrm{h} = M_\mathrm{A} = 60$ GeV and $M_\mathrm{h} = 50$ and $M_\mathrm{A} = 70$ GeV. Exclusion limits in the $(M_\mathrm{h}, M_\mathrm{A})$ plane are derived for values of $\eta' = 1.6$, $\eta' = 1.0$ and $\eta' = 0.5$, where $\eta' = \eta \cdot \mathcal{B}(\mathrm{hA} \rightarrow \mathrm{q\bar{q}q\bar{q}})$. They are shown in Figure 9. The upper limit on η' is also given as function of $(M_\mathrm{h} + M_\mathrm{A})/2$ assuming $M_\mathrm{h} = M_\mathrm{A}$ in Figure 10. The lower mass limit obtained at $\eta' = 1.0$ is $M_{\mathrm{h,A}} > 64$ GeV.

The hA $\rightarrow \tau^+\tau^-\mathrm{b}\bar{\mathrm{b}}$ final state

The selection is the same as described in Ref. [14]. A kinematic fit is performed to determine the invariant masses of the $\mathrm{b}\bar{\mathrm{b}}$ jets and of the tau leptons applying constraints to conserve energy and momentum. A discriminant variable is constructed from the probabilities that the two hadronic jets originate from b quarks and the probabilities to measure the masses obtained from the fit in case of the given mass hypothesis. The distribution of the discriminant variable is shown in Figure 11 for the hypotheses ($M_{\mathrm{b}\bar{\mathrm{b}}}$, $M_{\tau^+\tau^-}$)=(70,70)GeV and (60,80)GeV. No signal is seen, and upper limits on the masses are derived in the $M_{\tau^+\tau^-}$ vs. $M_{\mathrm{b}\bar{\mathrm{b}}}$ plane for $\eta' = 1.0$, $\eta' = 0.3$ and $\eta' = 0.15$, where $\eta' = \eta \cdot \mathcal{B}(\mathrm{hA} \rightarrow \tau^+\tau^-\mathrm{b}\bar{\mathrm{b}})$ as shown in Figure 12. The upper limit on η' as function of $(M_A + M_h)/2$ is shown in Figure 13 for $M_{\tau^+\tau^-}$=$M_{\mathrm{b}\bar{\mathrm{b}}}$. At $\eta' = 1.0$ scalar particle production is excluded up to a mass of 86 GeV.

The hA $\rightarrow \mathrm{q}\bar{\mathrm{q}}\tau^+\tau^-$ final state

The selection is the same as for the hA $\rightarrow \tau^+\tau^-\mathrm{b}\bar{\mathrm{b}}$ final state. The final discriminant is calculated using only the dijet and $\tau^+\tau^-$ masses and comparing their sum and difference with the mass hypothesis. The distributions of $(M_{\mathrm{b}\bar{\mathrm{b}}}+M_{\tau^+\tau^-})/2$ for the hypotheses ($M_{\tau^+\tau^-}$, $M_{\mathrm{q}\bar{\mathrm{q}}}$)=(70,70)GeV and (60,80)GeV are shown in Figure 14. No significant excess of data is observed. Using $\eta' = \eta \cdot \mathcal{B}(\mathrm{hA} \rightarrow \mathrm{q}\bar{\mathrm{q}}\tau^+\tau^-)$, upper limits on the masses are determined for $\eta' = 1.0$, $\eta' = 0.3$ and $\eta' = 0.15$ and shown in Figure 15 in the $M_{\tau^+\tau^-}$ vs. $M_{\mathrm{q}\bar{\mathrm{q}}}$ plane. The upper limit on η' as function of $(M_\mathrm{h} + M_\mathrm{A})/2$ is shown in Figure 16 for $M_{\tau^+\tau^-}$=$M_{\mathrm{q}\bar{\mathrm{q}}}$. The mass lower limit obtained at $\eta' = 1.0$ is 85 GeV.

References

[1] S.L. Glashow, Nucl. Phys. **22** (1961) 579;
S. Weinberg, Phys. Rev. Lett. **19** (1967) 1264;
A. Salam, “Elementary Particle Theory”, Ed. N. Svartholm, Stockholm, “Almquist and Wiksell” (1968), 367.

[2] P. W. Higgs, Phys. Lett. **12** (1964) 132; F. Englert and R. Brout, Phys. Rev. Lett. **13** (1964) 321; G. S. Guralnik *et al.*, Phys. Rev. Lett. **13** (1964) 585.

[3] John F. Gunion *et al.*, The Higgs Hunter’s Guide, (Addison Wesley, 1990).

[4] L3 Collaboration, B. Adeva and others, Nucl. Inst. Meth. **A 289** (1990) 35; J. A. Bakken and others, Nucl. Inst. Meth. **A 275** (1989) 81; O. Adriani and others, Nucl. Inst. Meth. **A 302** (1991) 53; B. Adeva and others, Nucl. Inst. Meth. **A 323** (1992) 109; K. Deiters and others, Nucl. Inst. Meth. **A 323** (1992) 162; M. Chemarin and others, Nucl. Inst. Meth. **A 349** (1994) 345; M. Acciarri and others, Nucl. Inst. Meth. **A 351** (1994) 300; G. Basti and others, Nucl. Inst. Meth. **A 374** (1996) 293; A. Adam and others, Nucl. Inst. Meth. **A 383** (1996) 342.

[5] P. Janot, *The HZHA Generator* in G. Altarelli, T. Sjöstrand, F. Zwirner,*Physics at LEP2*, CERN 96-01, 1996, vol. 2, p.309, version 3, released in December 1999, http://alephwww.cern.ch/janot/Generators.html.

[6] T. Sjöstrand, "PYTHIA", Preprint TH/93-7112, CERN, 1993, Revised August 1995; T. Sjöstrand, Comp. Phys. Comm. **82** (1994) 74.

[7] M. Skrzypek *et al.*, Comp. Phys. Comm. **94** (1996) 216; M. Skrzypek *et al.*, Phys. Lett. **B 372** (1996) 289.

[8] S. Jadach and B. F. L. Ward and Z. Wąs, Comp. Phys. Comm. **66** (1991) 276.

[9] R. Engel, Z. Phys. **C 66** (1995) 203; R. Engel and J. Ranft and S. Roesler, Phys. Rev. **D 52** (1995) 1459.

[10] F. A. Berends and R. Pittau and R. Kleiss, Comp. Phys. Comm. **85** (1995) 437.

[11] R. Brun *et al.*, "GEANT 3", CERN DD/EE/84-1, Revised 1987.

[12] H. Fesefeldt, "GHEISHA", Preprint PITHA 85/02, RWTH Aachen, 1985.

[13] L3 Collab., M. Acciarri *et al.*, Phys. Lett. **B 461** (1999) 376.

[14] L3 Collab., M. Acciarri *et al.*, Phys. Lett. **B 471** (1999) 321.

center-of-mass energy	$\int$ Ldt , pb^-1
189	176.4
192	29.7
196	83.7
200	82.8
202	37.0

Table 1: The integrated luminosities collected by L3 at different center-of-mass energies.

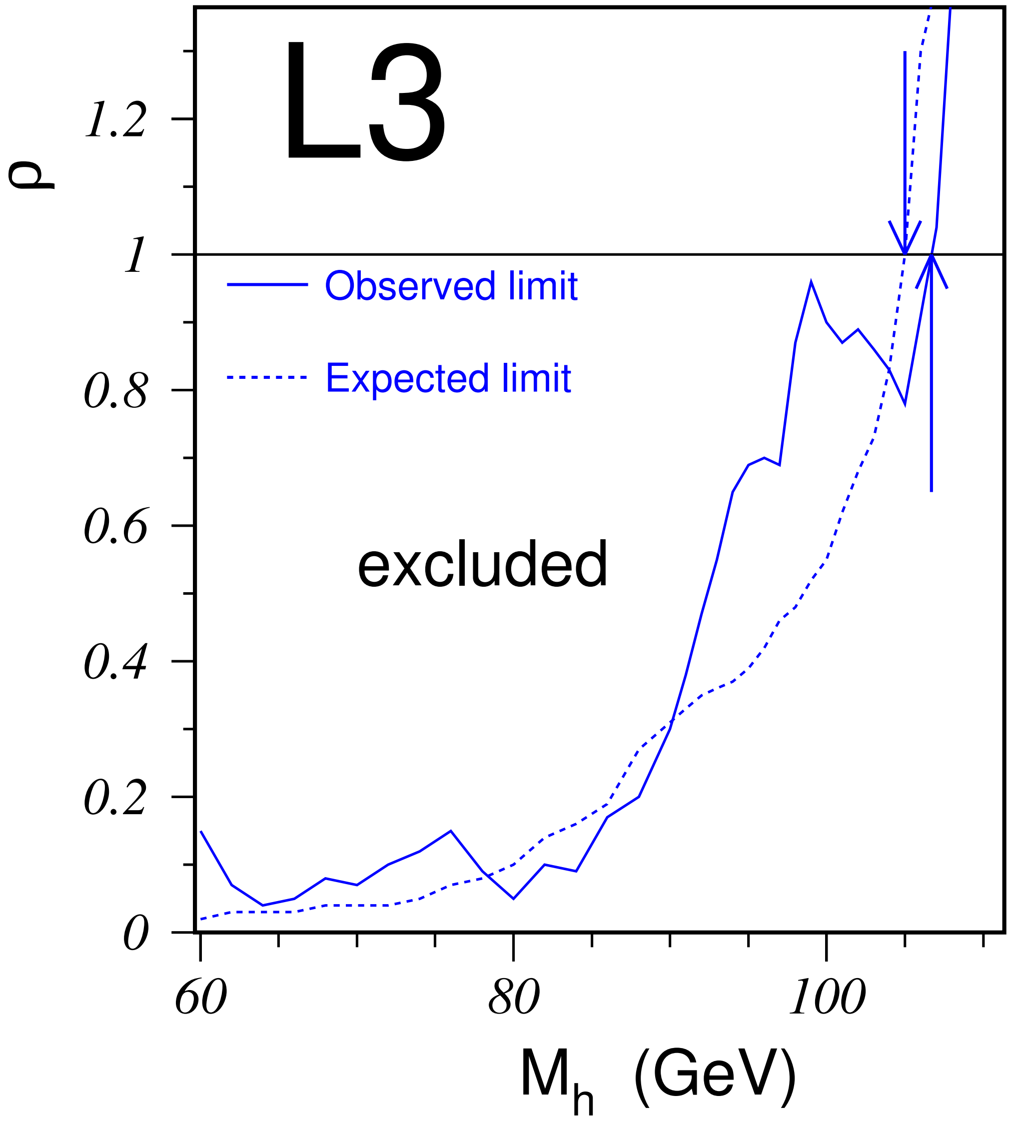

Figure 1: The 95% exclusion limit of the parameter ρ as function of M_{h}. At $\rho = 1$ the exclusion curve represents the M_{h} limit within SM.

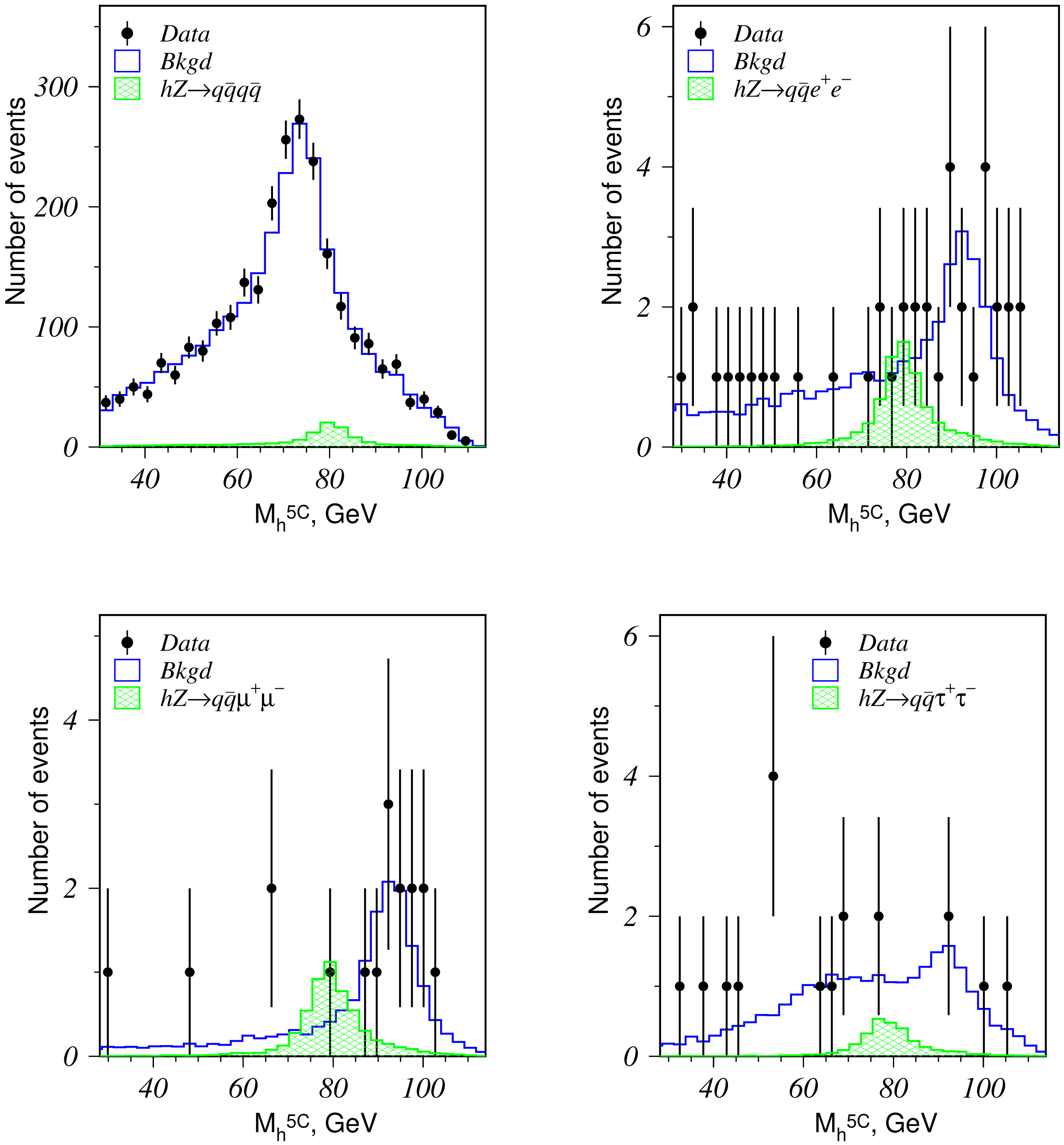

Figure 2: The distribution of the invariant mass of the two jets assigned to the decay $\mathrm{h} \rightarrow q\bar{q}$. Top left for the decay $\mathrm{hZ} \rightarrow \mathrm{q\bar{q}q\bar{q}}$, top right for $\mathrm{hZ} \rightarrow \mathrm{q\bar{q}e^+e^-}$, bottom left for $\mathrm{hZ} \rightarrow \mathrm{q\bar{q}}\mu^+\mu^-$ and bottom right for $\mathrm{hZ} \rightarrow \tau^+\tau^-\mathrm{q\bar{q}}$. Points are data, the open histogram the background from SM processes and the hatched histogram the expectation from a scalar particle h with mass of 80 GeV assuming g_{hZZ} equal to g^{SM}_{hZZ}.

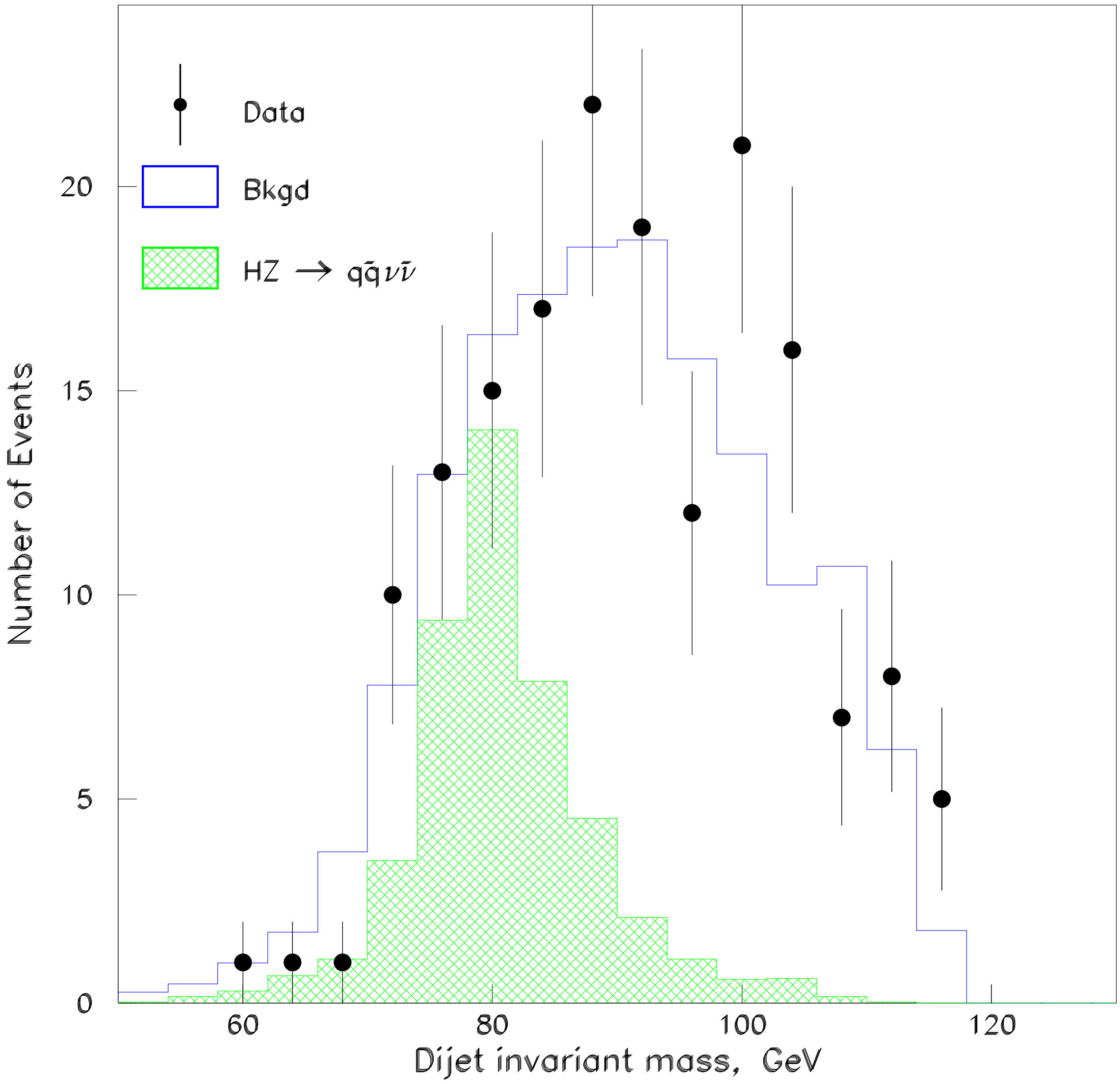

Figure 3: The distribution of the invariant mass of the two jets for hZ $\rightarrow$ $q\bar{q}\nu\nu$. Points are data, the open histogram the background from SM processes and the hatched histogram the expectation from a scalar particle h with mass of 80 GeV assuming $g_{\rm hZZ}$ equal to $g^{SM}_{\rm hZZ}$.

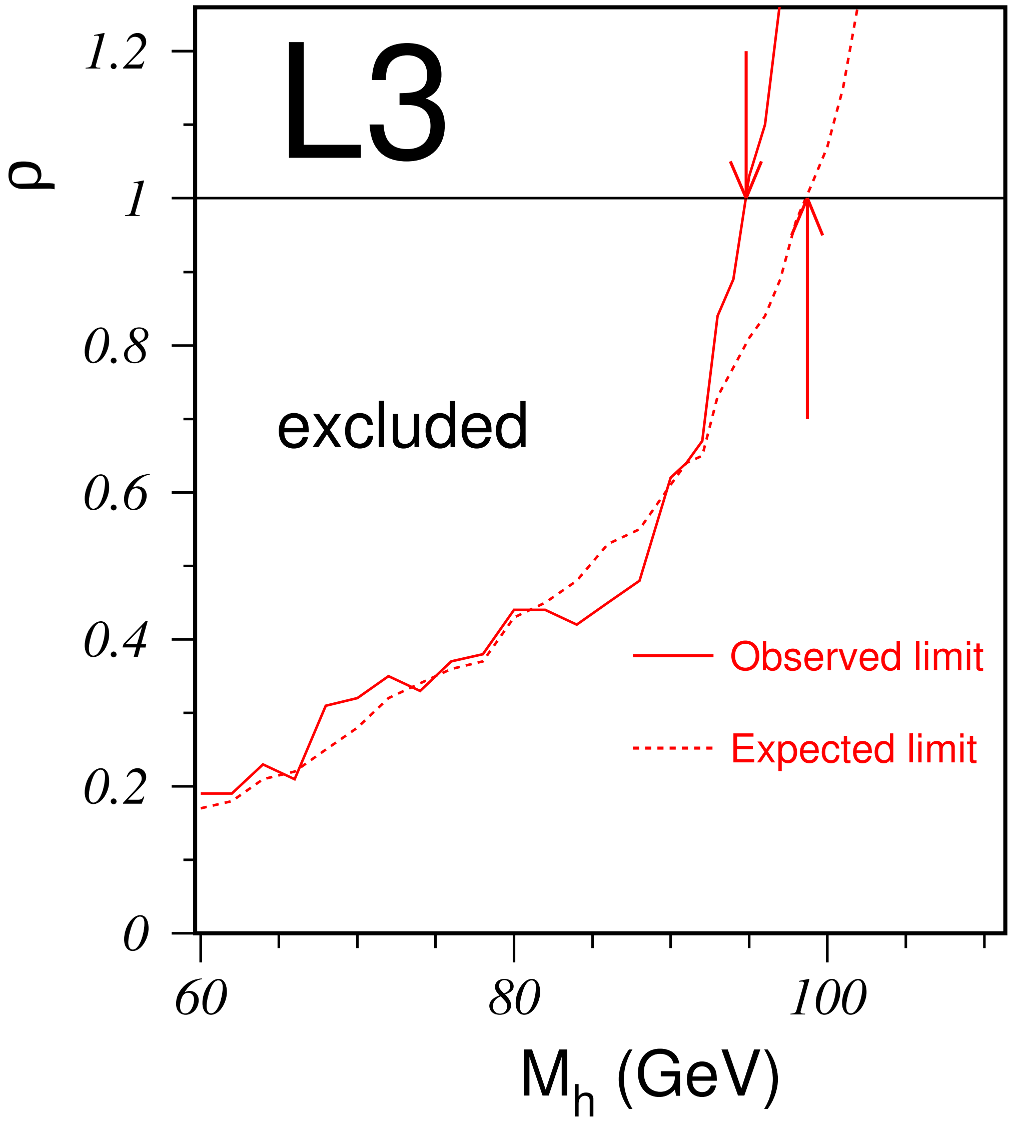

Figure 4: The 95% exclusion limit of the parameter ρ as function of M_{h} for $\mathrm{hZ} \rightarrow \mathrm{q\bar{q}f\bar{f}}$.

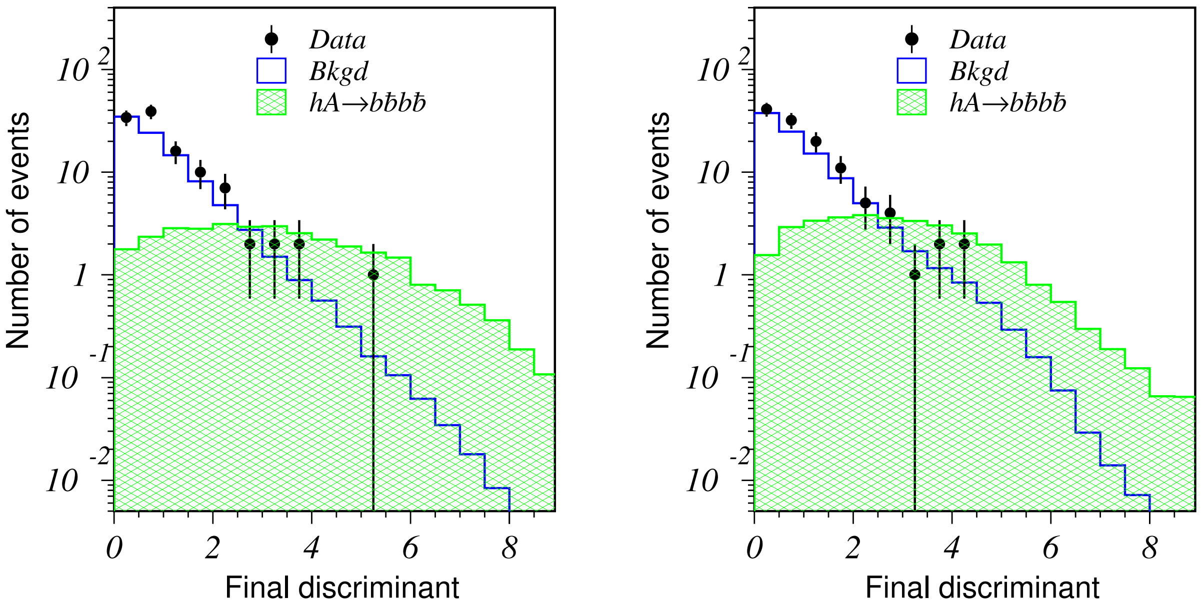

Figure 5: Examples of the distribution of the discriminant to separate hA $\rightarrow$ $\mathrm{b\bar{b}b\bar{b}}$ from the SM background. The points are data, the full line the SM background and the hatched histogram is the expectation for a signal with $M_{\mathrm{h}} = M_A = 75$ GeV (left) and M_{h} =65 GeV,M_{A} = 85 GeV (right) assuming η'=1.0.

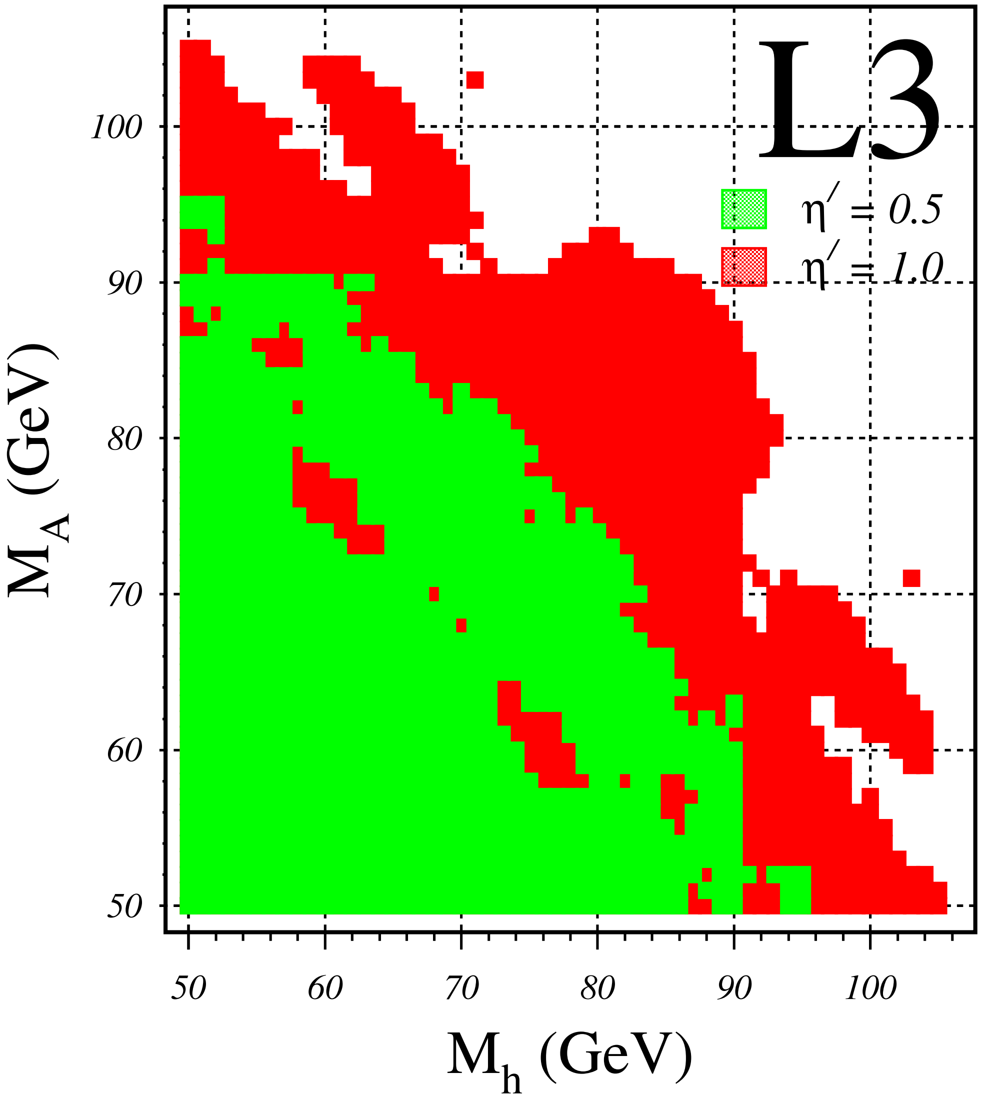

Figure 6: The 95% C.L. excluded region for the production of hA $\rightarrow \mathrm{b\bar{b}b\bar{b}}$ in the $(M_{\mathrm{A}}, M_{\mathrm{h}})$ plane for the assumptions $\eta' = 0.5$ (light grey area) and $\eta' = 1.0$ (dark grey area)

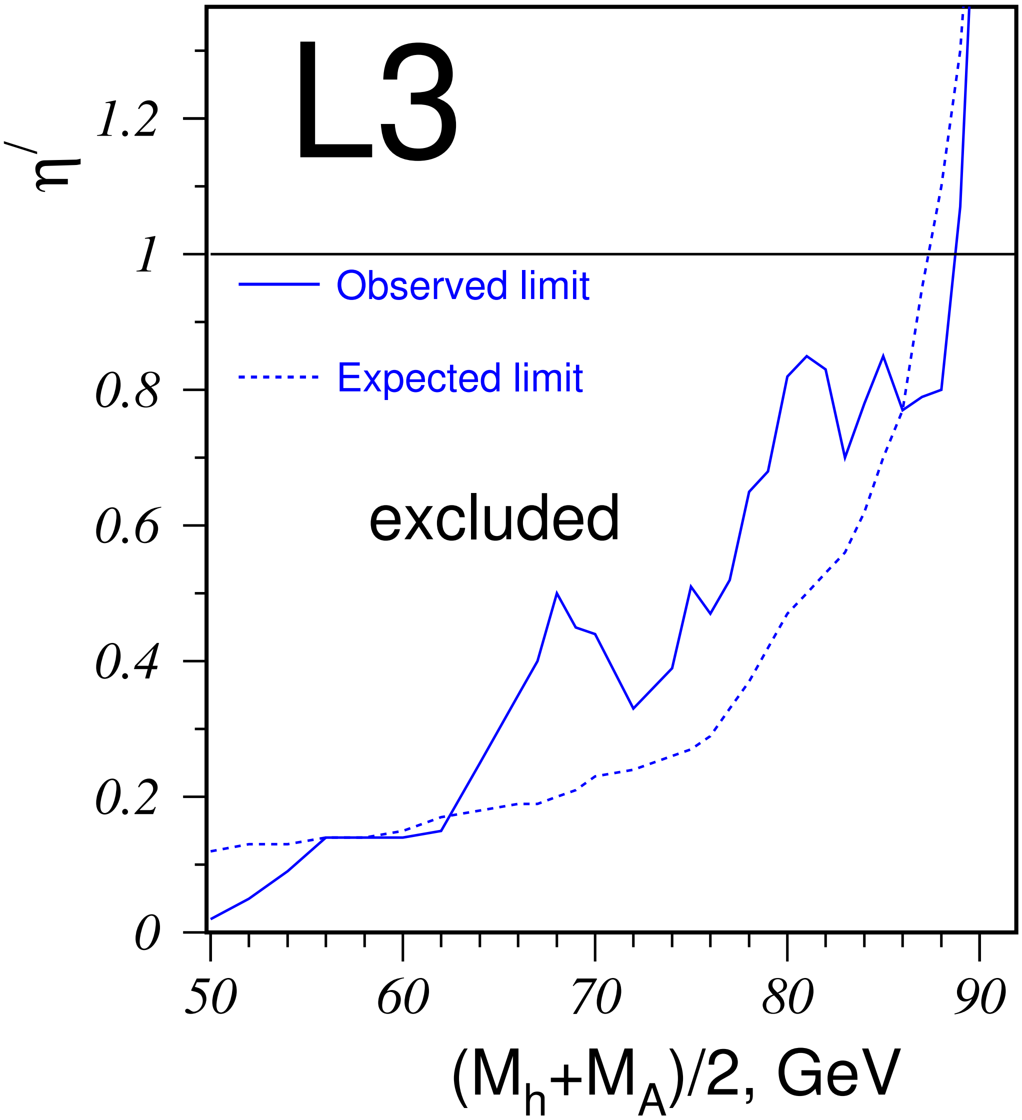

Figure 7: Limit on η' for hA $\rightarrow$ $\mathrm{b\bar{b}b\bar{b}}$ as function of $(M_\mathrm{A} + M_\mathrm{h})/2$ assuming $M_\mathrm{A} = M_\mathrm{h}$)

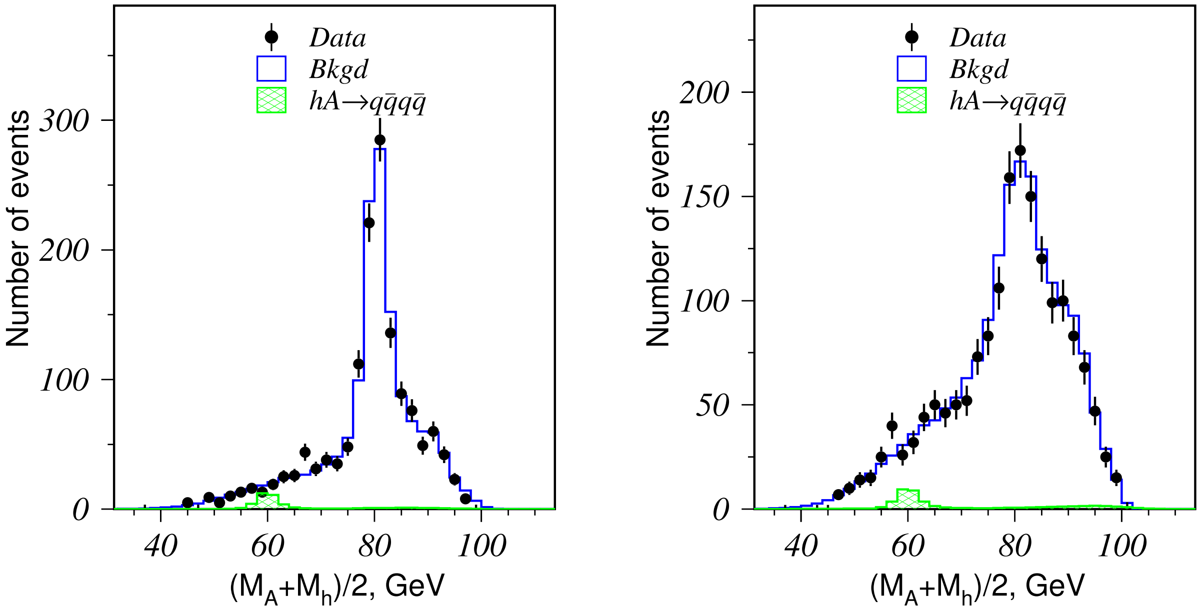

Figure 8: The sum of the dijet masses, $\frac{1}{2} = (M_{q\bar{q}} + M_{q'\bar{q}'})$ for the two hypotheses $M_A = M_h =$ 60 GeV and $M_A = 70$ and $M_h = 50$ GeV. The points are the data and the open histogram is the expectation from SM background. Also shown is the expectation for a signal with the masses given above assuming η'=1.0.

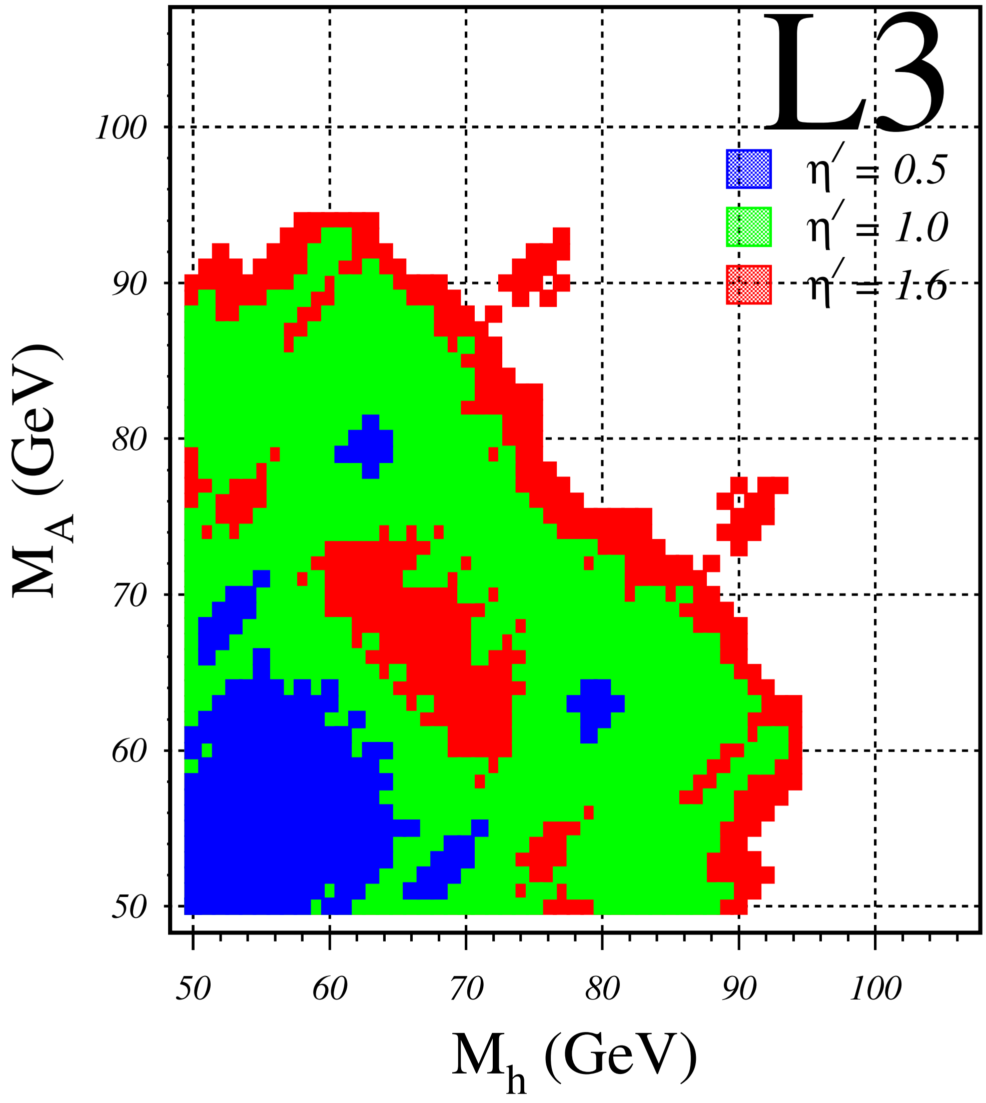

Figure 9: The 95% C.L. excluded region for the production of hA $\rightarrow$ q$\bar{\text{q}}$q$\bar{\text{q}}$ in the $(M_{\text{A}}, M_{\text{h}})$ plane for the assumptions $\eta' = 0.5$ (dark grey area), $\eta' = 1.0$ (light grey area) and $\eta' = 1.6$ (medium grey area)

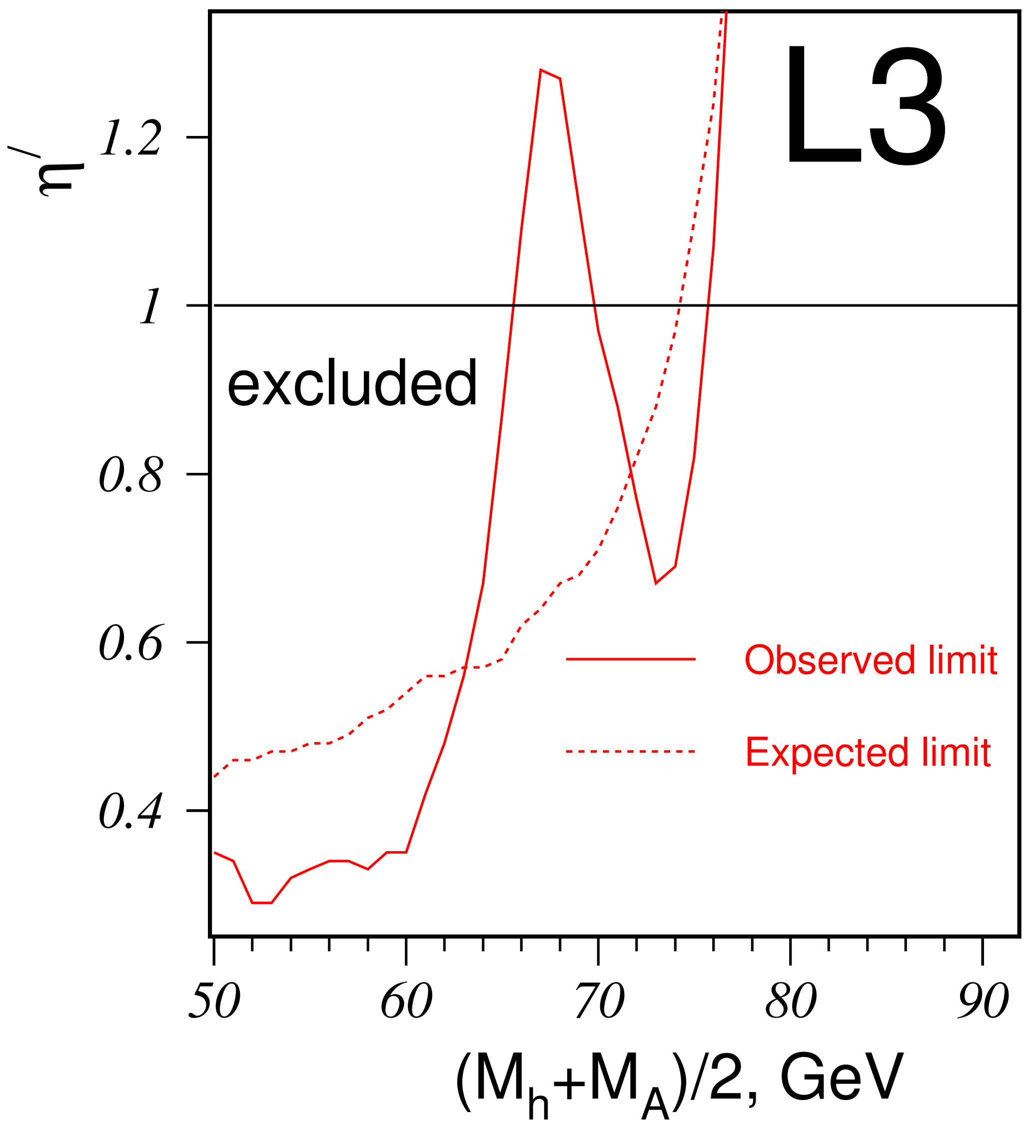

Figure 10: Limit on η' for hA $\rightarrow$ q$\bar{\mathrm{q}}$q$\bar{\mathrm{q}}$ as function of $(M_{\mathrm{A}} + M_{\mathrm{h}})/2$ assuming $M_{\mathrm{A}} = M_{\mathrm{h}}$)

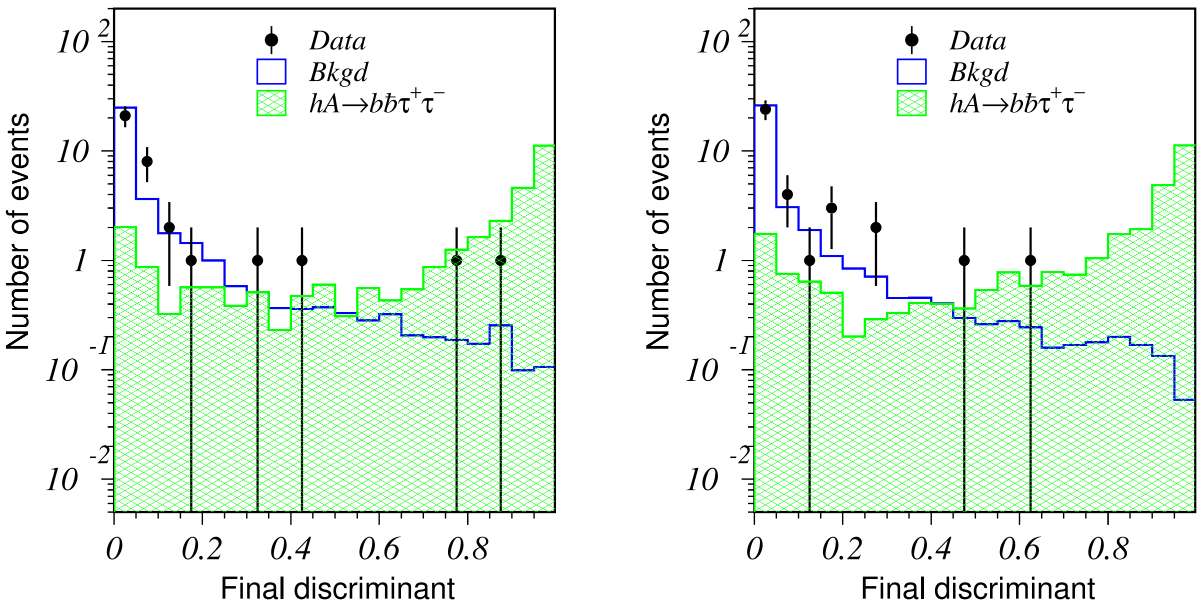

Figure 11: The discriminant distributions for the hA $\rightarrow \tau^+\tau^-\mathrm{b\bar{b}}$ final state for the assumptions $M_{\mathrm{b\bar{b}}}$= $M_{\tau^+\tau^-}$= 70 GeV and $M_{\mathrm{b\bar{b}}}$= 60 GeV and $M_{\tau^+\tau^-}$= 80 GeV. Points are data, the open histogram the background from SM processes and the hatched histogram the expectation from a scalar particle h with mass of 80 GeV under the assumption η'=1.0.

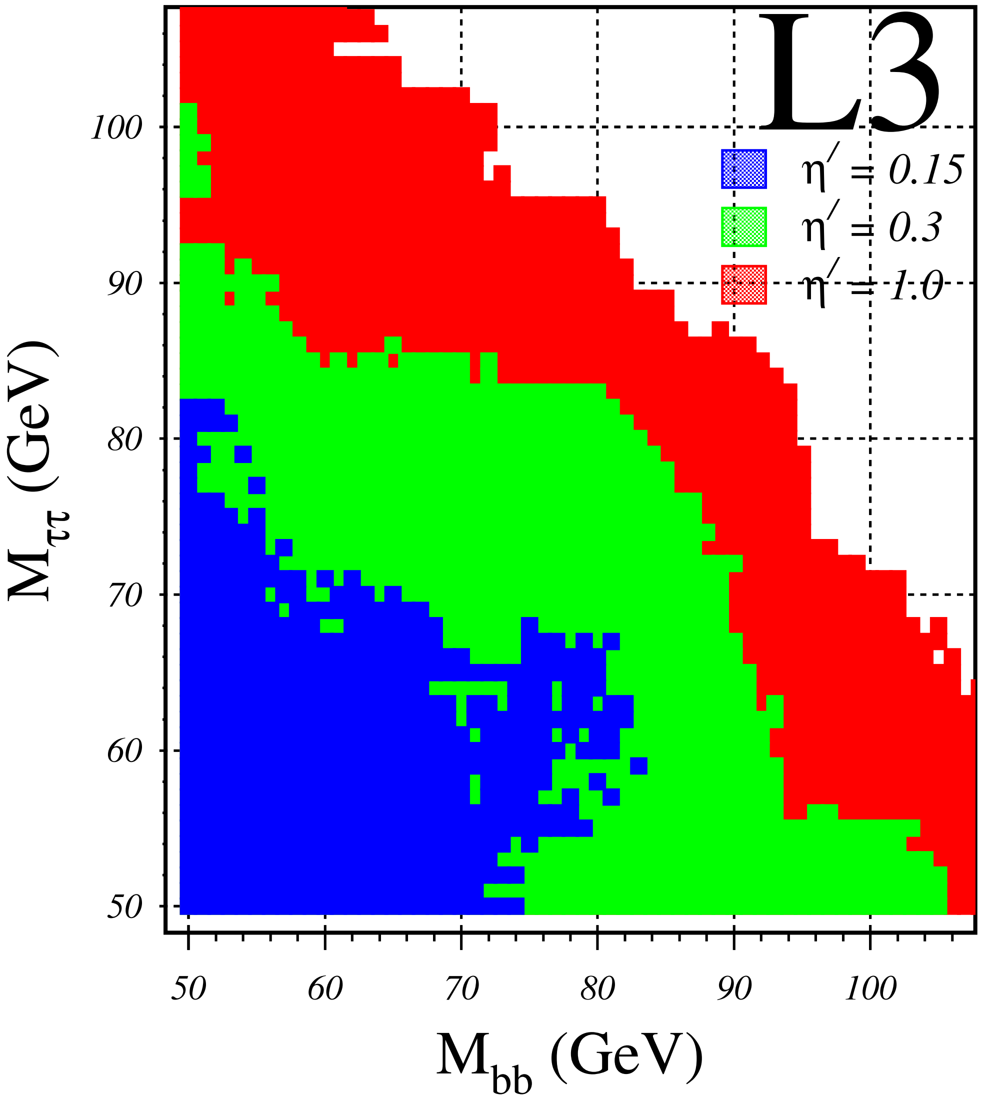

Figure 12: The 95% C.L. excluded region for the production of hA $\rightarrow \tau^+\tau^-b\bar{b}$ in the $(M_{\tau^+\tau^-}, M_{b\bar{b}})$ plane for the assumptions $\eta' = 0.15$ (dark grey area), $\eta' = 0.3$ (light grey area) and $\eta' < 1.0$ (medium grey area)

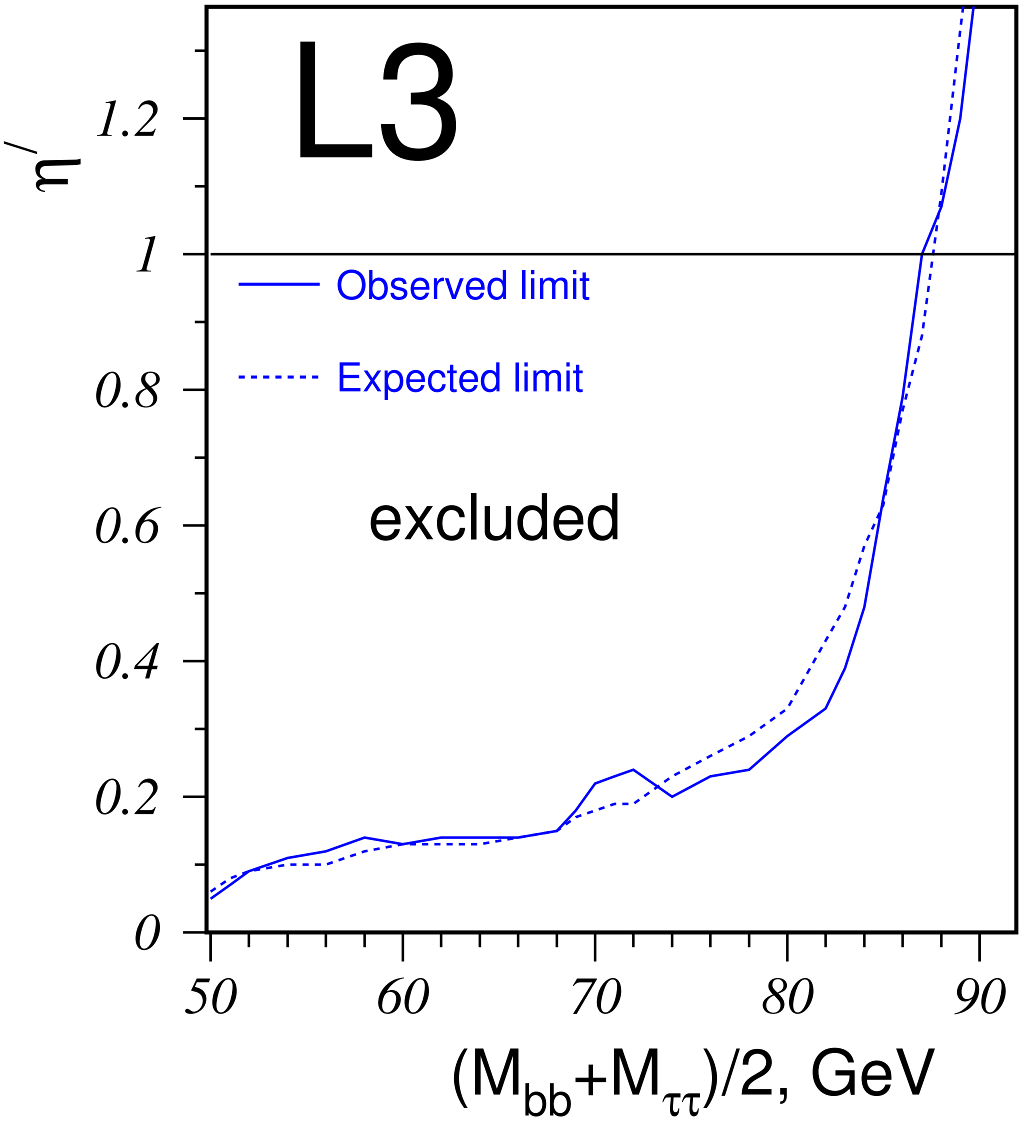

Figure 13: Limit on η' for $\mathrm{hA} \rightarrow \tau^+\tau^-\mathrm{b}\bar{\mathrm{b}}$ as function of $(M_\mathrm{A} + M_\mathrm{h})/2$ assuming $M_\mathrm{A} = M_\mathrm{h}$)

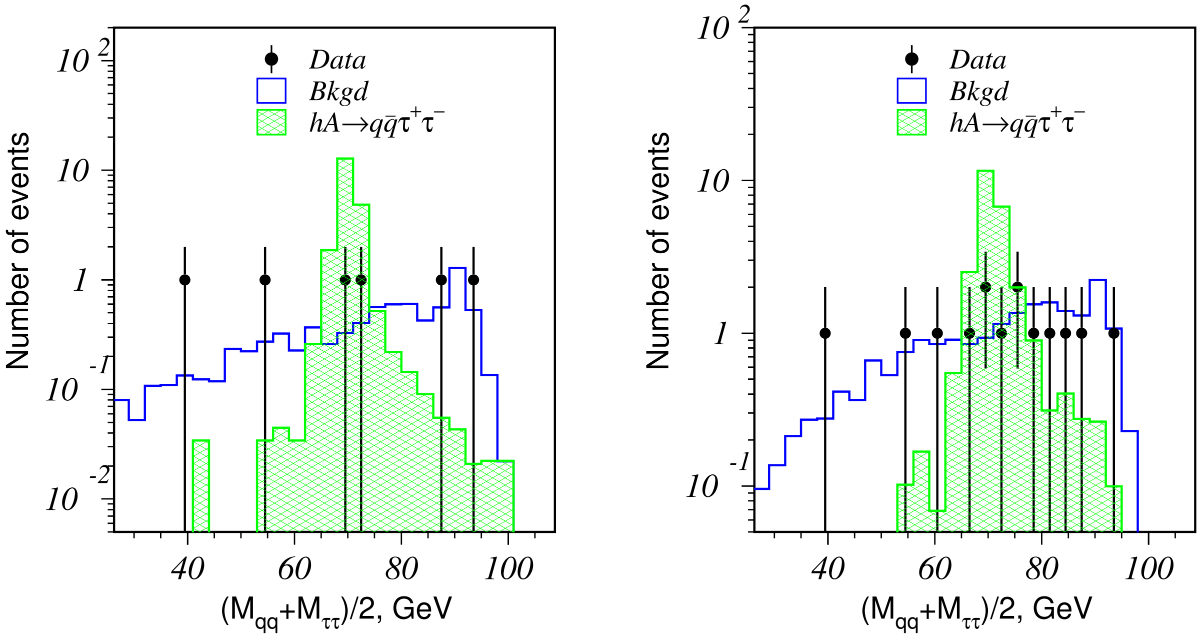

Figure 14: Examples of mass distributions for the hA $\rightarrow$ q$\bar{\text{q}}\tau^+\tau^-$ final state for the assumptions $M_{\text{q}\bar{\text{q}}}$= $M_{\tau^+\tau^-}$= 70 GeV and $M_{\text{q}\bar{\text{q}}}$= 60 GeV and $M_{\tau^+\tau^-}$= 80 GeV. Points are data, the open histogram the background from SM processes and the hatched histogram the expectation from a scalar particle h with mass of 80 GeV under the assumption η'=1.0.

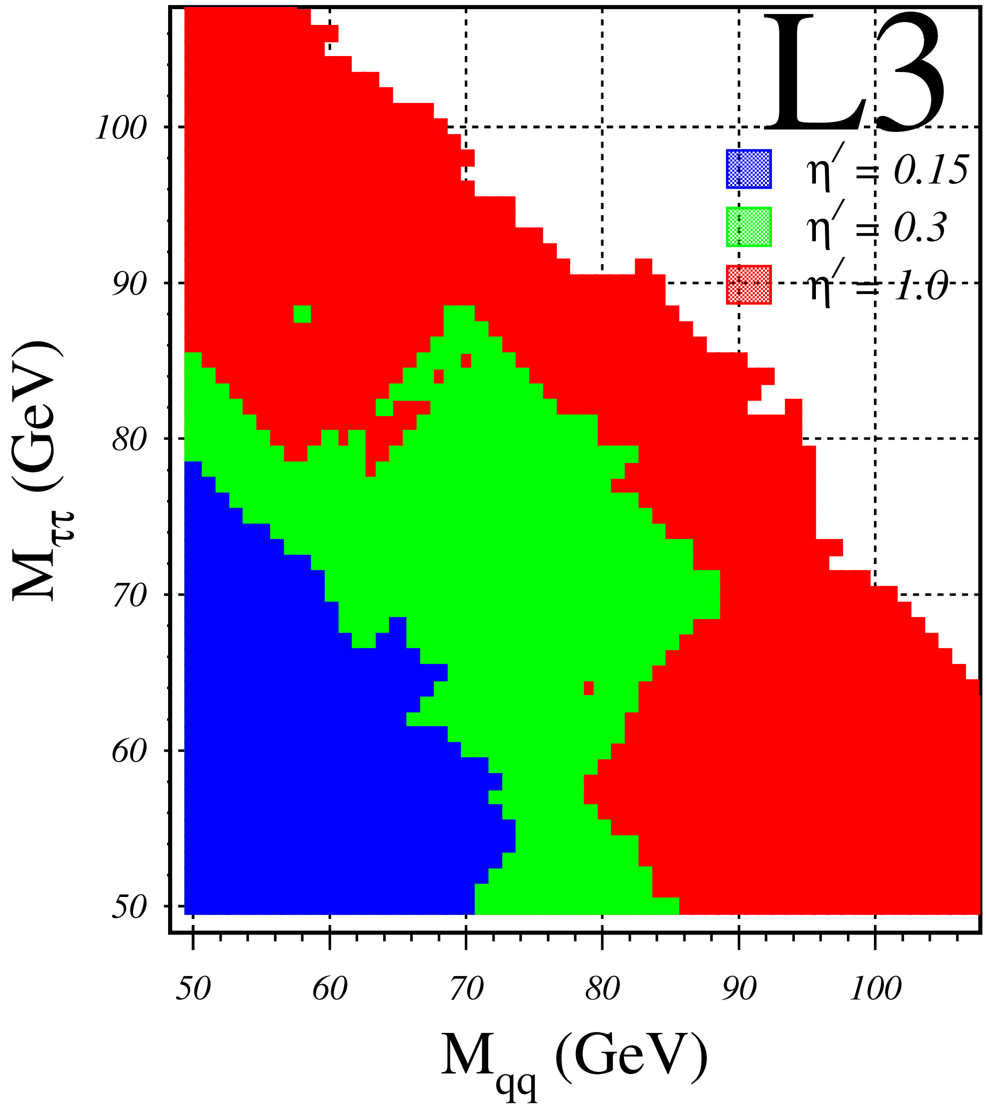

Figure 15: The 95% C.L. excluded region for the production of hA $\rightarrow$ q$\bar{\mathrm{q}}\tau^+\tau^-$ in the $(M_{\tau^+\tau^-}, M_{\mathrm{q}\bar{\mathrm{q}}})$ plane for the assumptions $\eta' < 0.15$ (dark grey area), $\eta' < 0.3$ (light grey area) and $\eta' < 1.0$ (medium grey area)

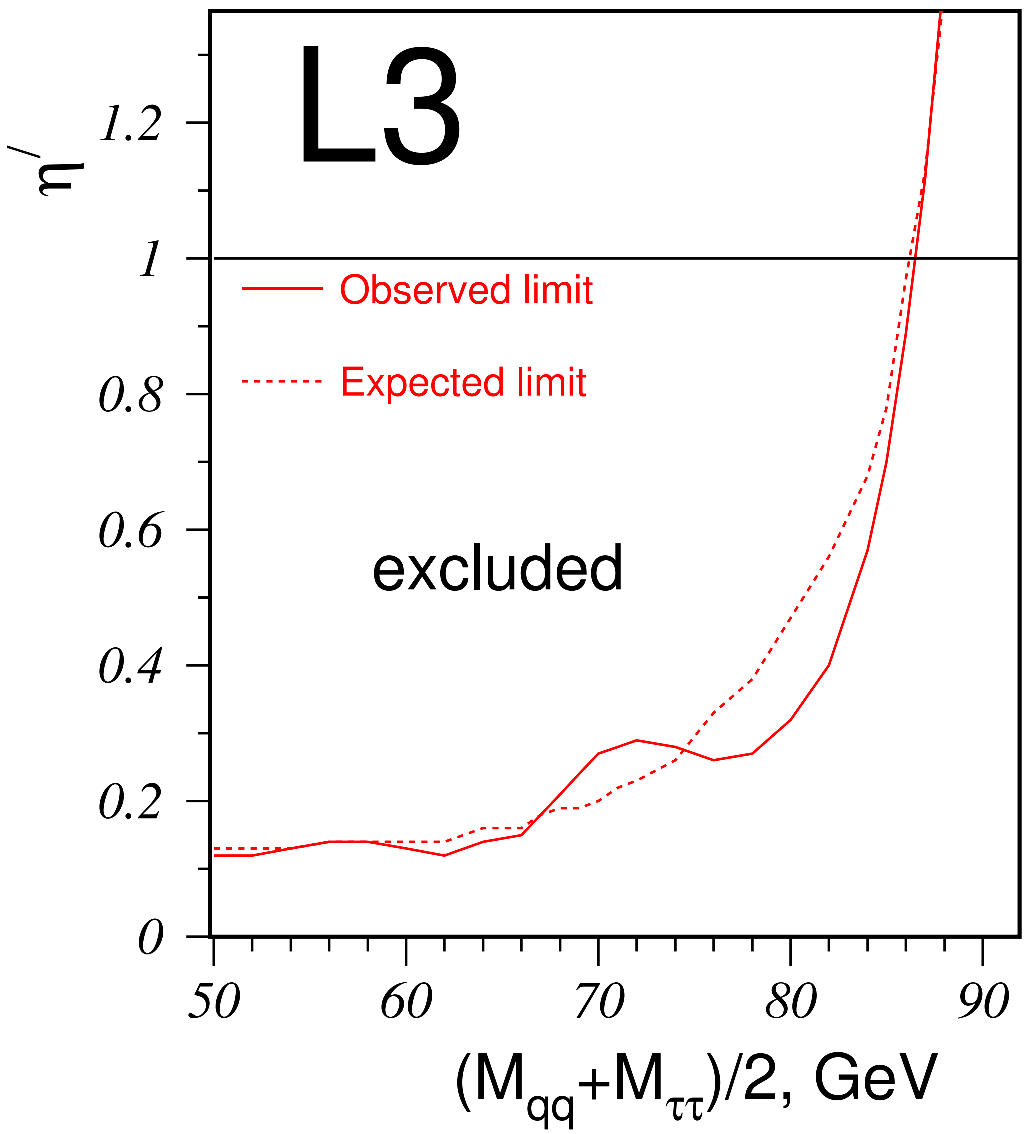

Figure 16: Limit on η' for hA $\rightarrow q\bar{q}\tau^+\tau^-$ as function of $(M_{\rm A} + M_{\rm h})/2$ assuming $M_{\rm A} = M_{\rm h}$